Innovative Food Science and Emerging Technologies 76 (2022) 102917

Contents lists available at ScienceDirect

Innovative Food Science and Emerging Technologies

journal homepage: www.elsevier.com/locate/ifset

Effects of electrolysed water combined with ultrasound on inactivation kinetics and metabolite profiles of *Escherichia coli* biofilms on food contact surface

Lin Zhao [a,c], Chieng Ning Poh [b], Jiaying Wu [a,c], Xue Zhao [a,c], Yun He [a,c], Hongshun Yang [a,c,*]

[a] Department of Food Science and Technology, National University of Singapore, 117542, Singapore
[b] Dunman High School, Singapore 436895, Singapore
[c] National University of Singapore (Suzhou) Research Institute, 377 Lin Quan Street, Suzhou Industrial Park, Suzhou, Jiangsu 215123, PR China

ARTICLE INFO

Keywords:
Biofilm
Modelling
Metabolomics
NMR
Organic food
Stainless steel

ABSTRACT

This study aimed to better understand the overall metabolic responses of *Escherichia coli* biofilms to the combined stresses of ultrasound and low concentration acidic electrolysed water (LcAEW, free available chlorine: 4 mg/L). The inactivation kinetics of all *E. coli* strains (ATCC 25922, ATCC 35150 and ATCC 43895) were simulated well by the modified Weibull model (R^2: 0.81–0.97; RMSE: 0.04–0.71). By analysing metabolite profiles, ultrasound mainly disrupted nucleotide metabolism in *E. coli* cells within biofilms, as most intracellular nucleotide-related compounds (*e.g.,* uridine, ATP, ADP) showed decreased trend especially in ATCC 25922 and ATCC 35150. Increased contents of most amino acids and decreased contents of most carbohydrates were shown in all strains after LcAEW treatment. Under combined treatment, adaptive strategies like glutamate decarboxylase system and mixed acid fermentation were activated to different extents among the three strains. These findings revealed that NMR-based metabolomics technology is promising in identifying strain-specific metabolic responses of biofilms to different antimicrobial treatments, providing guidance for future mechanism studies related to food contact surface sanitisation.

1. Introduction

Biofilms can be defined as aggregates of microbial cells embedded within a self-secreted matrix called extracellular polymeric substances (EPS) (Cui, Li, Abdel-Samie, Surendhiran, & Lin, 2021). In the food industry, once foodborne pathogens attach to food contact surfaces (*e.g.,* work benches, storage tanks, kitchen wares), they are very likely to form biofilms as their survival strategy, leading to subsequent food spoilage and even foodborne diseases (Tan & Karwe, 2021; Yemmireddy & Hung, 2015). Considering an estimated 65–80% of human microbial infections are caused by biofilms (Jamal et al., 2018), finding an effective biofilm removal strategy is of great significance in food contact surface sanitisation.

Many chemical sanitisers are applied in the food industry for sanitising food contact surfaces currently. However, fewer chemical sanitisers can be used for organic food production due to the strict rules (Adhikari, Syamaladevi, Killinger, & Sablani, 2015). For example, U.S. National Organic Program regulates that the residual chlorine levels should not exceed 4 mg/L when chlorine-based materials are used to sanitise organic food contact surfaces (NOP 5026, 2011). Compared to the conventional chemical reagents, low concentration acidic electrolysed water (LcAEW, free available chlorine (FAC): 4 mg/L), yielded from water and salt electrolysis, can meet organic operation standards due to its environmentally friendly nature and safe characteristic. As one of the emerging sterilisation agents in food industry in recent decades, LcAEW exhibited significant antimicrobial effect on planktonic cells in our previous study, but when used on biofilms, it might become less effective like other chemical sanitisers due to its limited penetration into deep layers of biofilm (Zhao, Zhang, & Yang, 2017; Zhao, Zhao, Phey, & Yang, 2019). Therefore, to achieve an effective detachment and inactivation of microbial biofilms from food contact surfaces, another method needs to be combined with LcAEW and ultrasound could be one choice.

Ultrasound-involved emerging strategies have gained increasing attention recently. As a strong physical processing method, ultrasound can destroy the structure of microbial communities effectively and remove the biofilms from food contact surfaces. However, the

* Corresponding author at: Department of Food Science and Technology, National University of Singapore, 117542, Singapore.
E-mail address: fstynghs@nus.edu.sg (H. Yang).

https://doi.org/10.1016/j.ifset.2022.102917
Received 21 August 2021; Received in revised form 22 December 2021; Accepted 3 January 2022
Available online 7 January 2022

bactericidal effect of ultrasound alone is very limited, as the thick and soft capsule layer of bacteria can dampen the mechanical effects of ultrasound (Gao, Lewis, Ashokkumar, & Hemar, 2014). Fortunately, when combined with chemical disinfectants to treat biofilms, ultrasound can expose inner cells to the disinfectants and promote the permeability of chemical disinfectants into the biofilms by mechanical oscillation, helping chemical sanitisers to achieve an enhanced bactericidal effect on biofilms (Bang, Park, Kim, Rahaman, & Ha, 2017). In previous studies, commonly used sanitisers like sodium hypochlorite, benzalkonium chloride and quaternary ammonium were combined with ultrasound to treat biofilms formed on different food contact surfaces like stainless steel, polystyrene and polyvinyl chloride, causing 60–90% reduction of viable cells and achieving synergistic bactericidal efficacy than each used alone (Berrang, Frank, & Meinersmann, 2008; Lee, Kim, & Ha, 2014; Torlak & Sert, 2013). However, although the combination of electrolysed water and ultrasound has been widely used in food preservation as an effective sanitising method in recent years (Ding et al., 2015; Wu et al., 2018), there are few available information about their effects on the inactivation kinetics and metabolic changes of biofilms on food contact surface.

A variety of mathematical models have been evaluated to describe the antibacterial effect over the treatment time, such as first-order kinetic model fitting linear reduction curve and Weibull, Baranyi, Gompertz and Huang models fitting nonlinear reduction curve (Baranyi & Roberts, 1995; Huang, 2009). However, the inactivation kinetics of ultrasound and LcAEW combination against biofilms on food contact surface has not been generally characterised by mathematical models. Moreover, beneath the reduction surface, the overall metabolite changes of biofilms after this combined treatment have not been investigated so far. Metabolomics, as supplementary to proteomics and genomics, can help people figure out how a series of actual physiological processes change in living organisms, considering it is able to focus on low-molecule-weight metabolites produced by the cells (Smart, Aggio, Van Houtte, & Villas-Bôas, 2010). Although there are multiple studies on the comparison of metabolite profiles between biofilm and their planktonic counterparts during biofilm formation process (Hamilton et al., 2009; Lu, Que, Wu, Guan, & Guo, 2019), the metabolic changes within established biofilms during external sanitising treatments have not been fully understood, let alone the strain-specific biofilm metabolic responses to ultrasound and LcAEW.

Therefore, in this study, the inactivation kinetics of three separate strains of *Escherichia coli* biofilms attached on stainless steel coupons were described quantitatively after ultrasound and LcAEW combined treatment. Moreover, the metabolomic variations of each biofilm induced by the two stresses were also identified by using nuclear magnetic resonance (NMR) spectroscopy, providing more fundamental understanding of cellular behaviours to hostile environments. Based on the dynamics study and the metabolic profiling analysis, this study would expand our knowledge on the biofilm-specific response mechanisms and provide effective antibiofilm strategies to the organic food industry.

2. Materials and methods

2.1. Bacterial strain and culture conditions

Three *E. coli* strains (*E. coli* O157:H7 ATCC 35150, *E. coli* O157:H7 ATCC 43895 and their non-pathogenic counterpart, *E. coli* ATCC 25922), obtained from Department of Food Science & Technology, National University of Singapore, were used in this study. After taken out from −80 °C freezer, the lyophilised culture of each strain was transferred to 5 mL of sterile tryptic soy broth (TSB, Oxoid, UK) for an 18–24 h resuscitation in a 37 °C incubator with 100 rpm rotation, following a streak plating on tryptic soy agar (TSA, Oxoid, UK) to get a single colony. After an overnight incubation at 37 °C, the individual colony was subcultured in TSB again and the working suspension of each strain was obtained after two consecutive transfers.

2.2. Biofilm formation

Preparation of *E. coli* biofilms was conducted as described previously with some modifications (Ayebah, Hung, Kim, & Frank, 2006; Yang, 2012). The working suspension at a concentration of 10^9 CFU/mL in 5 mL TSB was centrifuged (8000 ×*g*, 20 °C, 5 min), and the obtained pellets were added 5 mL 0.1% peptone water (PW) and centrifuged again. After this operation was repeated twice, the final bacteria cells were obtained and resuspended in 5 mL PW. One millilitre of the suspension was mixed well with 9 mL diluted TSB (dTSB, 1:10) in a petri dish, with sterilised stainless steel coupons (diameter: 1 cm; thickness: 0.7 mm; type: 430) immersed inside. The bacteria on the surface of coupons were cultured in an incubator at 25 °C for 4 h to allow adhesion, after which the suspensions were discarded and the coupons were gently rinsed in 10 mL PW to remove the loose cells. Then the coupons were transferred to 10 mL new dTSB for further biofilm growth at 25 °C. After a 48-h incubation, the spent medium was discarded, and the coupons were submerged in 10 mL fresh dTSB for another 24-h incubation to allow further biofilm growth. After above incubations, the initial biofilm populations of each strain on stainless steel coupons could reach ~7.0 log CFU/coupon, which were ready for following treatments.

2.3. Treatment of biofilms on the coupons

After the rinsed coupons were dried for 2 h in a laminar flow biosafety cabinet, 20 pieces of them were separately immersed in sterile 25 mL beakers containing 10 mL LcAEW (FAC: 4 mg/L), which was obtained by diluting anolyte from a 0.9% NaCl-electrolysis device (ROX-10WB, Hoshizaki Singapore Pte Ltd). The pH and oxidation reduction potential (ORP) values of used LcAEW were measured in a range of 4.0 ± 0.1 and 940.5 ± 10.0 mV, respectively based on previous methods (Chen, Chen, Chang, Huang, & Chen, 2021). A chlorine test kit (Merck, Darmstadt, Germany), pH meter (Thermo Orion pH meter, Waltham, USA) and ORP meter (HM Digital ORP-200, Culver City, USA) were used to test FAC, pH and ORP value, respectively. The same steps were applied for the control group of using 10 mL sterile deionised water (DW). Ultrasound alone or combined treatments were applied by putting the beakers (containing DW or LcAEW) in an ultrasonic cleaning unit (Elmasonic S 30 H, Siegen, Germany), with a settled frequency of 37 kHz and effective power of 80 W. After 0–5 min treatment, the collected coupons at different time points were immersed in 5 mL neutralising buffer (containing 5 g/L sodium thiosulfate) for 5-min neutralisation, to neutralise residual chlorine before microbial analysis (Luu, Chhetri, Janes, King, & Adhikari, 2021). Then the adherent cells on coupons were knocked down by 2 g glass beads (0.2 mm) on a vibrating vortex at maximum speed in 5 mL phosphate-buffered saline (PBS, pH 7.2) for 1 min. This method was proved to be effective to detach biofilm cells from stainless steel coupons previously (Kang, Lee, & Kang, 2021).

2.4. Cell enumeration

The detached cells from coupons were decimally diluted by PBS and 0.1 mL of each diluent was spread onto TSA plates. The colonies on the plates were enumerated after incubating at 37 °C for 24 h and expressed as log CFU/coupon. For microorganisms transferred to suspension after each treatment, 0.5 mL of the suspension in the beakers was mixed well with 0.5 mL neutralising buffer for 5-min neutralisation. The survival population in the suspension was counted following the same steps of dilution and plating as mentioned above and shown as log CFU/mL.

2.5. Mathematical modelling of antibiofilm effect

Three inactivation models were employed to describe the removal kinetics of *E. coli* biofilms on coupons under different treatments:

Linear model: $y = kx$, where y is the antibiofilm effect in log CFU/coupon, x is the time in min, k is the linear regression parameter.

Modified Weibull model: $y = \frac{1}{2.303}\left(\frac{x}{\alpha}\right)^{\beta}$, where α is the scale factor, β is the shape parameter. Moreover, T_R (the time needed for 90% biofilm reduction) was calculated based on the following equation: $T_R = \alpha(2.303)^{\frac{1}{\beta}}$, to evaluate Weibull parameters (Liu, Jin, Feng, Yang, & Fu, 2019).

Reduced Baranyi model: $y = \mu_{max}x + \ln[\exp(-\mu_{max}x) + \exp.(-h) - \exp.(-\mu_{max}x - h)]$, where μ_{max} is the maximum specific growth rate, h is the physiological state of the bacterium in log CFU/coupon.

The goodness of each model fitting was evaluated by the coefficient of determination (R^2) and the Residual Mean Square Error (RMSE), which were obtained from MATLAB R2018a (The Mathworks, Inc., Natick, USA). In addition, the parsimony of each model was judged by Akaike Information Criterion (AIC), which was used for an overfitting determination and calculated as below:

$$AIC = n\ln(SSE) + 2p$$

where n is the number of data points used for modelling, SSE is the Sum of Squares for Error and p is the number of parameters used in each model.

2.6. Confocal laser scanning microscopy (CLSM) analysis

To visualise the biofilm structure after each treatment, CLSM analysis was conducted based on a reported method (Pang & Yuk, 2019). The biofilms on stainless steel coupons were stained with a LIVE/DEAD® *Bac*Light™ Viability Kit L-7007 (Molecular Probes™, Eugene, USA). After incubation at dark for 15 min, the coupons were examined immediately by an inverted FLUOVIEW® FV 1000 Laser Scanning Confocal Microscope (Olympus, Tokyo, Japan) with a 60× objective accompanied by a 488 nm and 543 nm argon laser for green and red excitation, respectively, in which BA 505–525 and BA 560 IF were two filters used for the green and red channel, respectively. Representative 3D CLSM images from each treatment group were processed using IMARIS 7.6 software (Bitplane AG, Zurich, Switzerland).

2.7. Extraction of biofilm metabolites

The biofilms on coupons after 5-min treatment were used to do the metabolomics analysis, according to a method described by Zhao, Zhao, Wu, Lou, and Yang (2019) with some modifications. Once the cells were detached from coupons after vortex in Section 2.3, they were washed by PBS twice and the collected pellets were dissolved in a mixture of equal volumes of PBS and acetonitrile, which was served as a metabolite extraction solution. Then the bacteria cells were broken down by an ultrasonic crusher with 25 cycles and each cycle included 5 s pulses and 10 s stops. After centrifugation (12,000 ×*g*, 4 °C, 10 min), the supernatant with metabolites was obtained and the solid residues were used for collecting a secondary supernatant by homogenising again in the same extraction solution with a vortex. The two supernatants were then combined and both the acetonitrile and water in it were removed by a rotary evaporator and then the metabolite extracts from the lysed cells were obtained. The dried samples were stored at −20 °C for further NMR analyses.

2.8. NMR spectroscopic analysis

The solid samples prepared for NMR analysis was dissolved in deuterated water (D_2O, 99.9%), and sodium 3-trimethylsilyl [2,2,3,3-d4] propionate (TSP, Sigma-Aldrich, USA) was added as an internal reference with a 0.005% concentration ratio, to help quantify the concentration of biofilm metabolites and calibrate the chemical shift. The mixture was centrifuged (12,000 ×*g*, 4 °C, 10 min) and 600 μL supernatants were transferred into 5-mm NMR tubes by pipette.

A Bruker DRX-500 NMR Spectrometer (Bruker, Rheinstetten, Germany) set at 25 °C was applied to conduct ^{1}H NMR measurements, with a use of Triple Inverse Gradient probe running at 500.23 MHz. The ^{1}H spectrum was obtained after setting the parameters needed in a first increment of NOESY pulse sequence, which were set as follows according to a previous report (Wu, Zhao, Lai, & Yang, 2021): recycle delay (2 s) − 90° (10 μs) − t_1 (6.5 μs) − 90° − t_m (100 ms) − 90° − acquisition (1.36 s). A continuous weak wave irradiation was joined during the period of both recycle delay and t_m to do a water suppression. Each spectrum consisted of 64 transients of 32 k data points with a 20-ppm spectral width. Furthermore, before Fourier transformation, an exponential window function with a 1-Hz broadening factor was used to transform all free induction decays. After 1D spectrum was gained via 4 dummy scans and 128 scans, a series of 2D ^{1}H-^{13}C heteronuclear single quantum coherence spectra (HSQC) of selected samples were obtained to identify the metabolite signal assignment. The F1 channel was assigned to test the ^{13}C spectra with a 180-ppm spectral width while the F2 channel was used to collect the ^{1}H spectra with a 10-ppm spectral width (Lavoine et al., 2014). All assays were done in triplicate.

2.9. Spectral processing and analysis

The obtained NMR spectra were subject to software TopSpin 4.0.3 (Bruker) for baseline correction and phase adjustment. The 2D ^{1}H-^{13}C NMR spectrum was used as an auxiliary means of metabolite identification cooperatively with 1D ^{1}H spectra. The chemical shift assignments were determined by referring to several databases, such as the *E. coli* Metabolome Database (http://www.ecmdb.ca/) and the Biological Magnetic Resonance Data Bank (http://www.bmrb.wisc.edu/).

Furthermore, the spectra were integrated into regions (0.5–10.0 ppm) with water region (4.74–4.78 ppm) excluded by using the software Mestrenova (Mestreab Research SL, Spain), which can normalise the peaks to the sum intensities with equal width of 0.004 ppm. The data sets were then subject to multivariate analysis using SIMCA software (version 14.0, Umetrics, Sweden), which can carry out the principal component analysis (PCA) and the orthogonal projection to latent structure discriminant analysis (OPLS-DA) sequentially, showing the separation of each data set and identifying the differences between control and combined treatments, respectively. All OPLS-DA models were further evaluated by the variable importance in projection (VIP), the fold change (FC) and the related *P* values in each pairwise comparison, to distinguish significantly changed metabolites that were susceptible to external treatments (Wang, Wu, & Yang, 2022). Lastly, metabolites with VIP > 1 were imported into MetaboAnalyst 5.0 (https://www.metaboanalyst.ca/) for metabolic pathway analysis, by referring to Kyoto Encyclopedia of Genes and Genomes (KEGG) database (https://www.genome.jp/kegg/pathway.html) accordingly.

2.10. Statistical analysis

All microbiological assays were conducted in triplicates and the bacterial count was calculated from duplicate plating at each data point. The results were expressed as mean value ± standard deviation. The data were analysed statistically by using analysis of variance (ANOVA) ($P < 0.05$) and the means comparisons among different treatment groups were achieved through the Duncan's multiple range test with an IBM SPSS statistical software (version 24; IBM Co., Armonk, NY, USA).

3. Results and discussion

3.1. Eradication effect of ultrasound and LcAEW on coupon and in suspension

The biofilm reduction curves fitted with different models on three *E. coli* strains under different treatments are shown in Fig. 1. There was little difference in reduction amount between LcAEW and control group for all *E. coli* biofilms, which is as expected since the cells in the inner

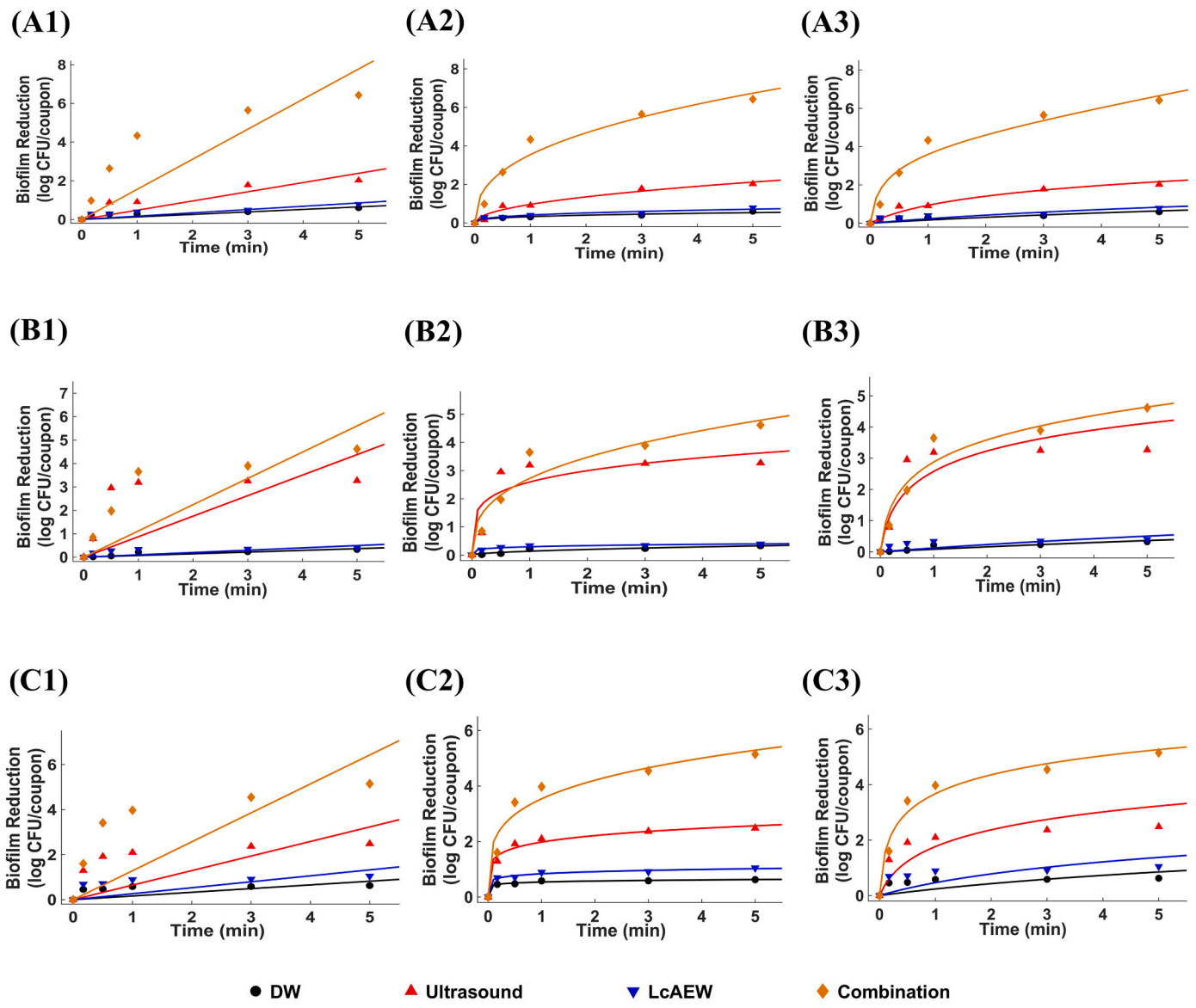

Fig. 1. Modelling of biofilm reduction on coupons under different treatments. A: ATCC 25922; B: ATCC 35150; C: ATCC 43895. A1, B1, C1: Linear model; A2, B2, C2: the modified Weibull model; A3, B3, C3: the reduced Baranyi model.

layer of biofilm are well-protected by the EPS structure against disinfectant penetration. However, through CLSM examination, a large quantity of cells of three strains under 5-min LcAEW treatment were stained red as shown in Fig. S1, indicating that the cells lost their membrane integrity to a certain extent but were still cultivable (Zhang, Pang, Seck, & Zhou, 2021). On the other hand, the loose cells of ATCC 25922 and ATCC 43895 transferred to suspension in LcAEW group could not be detected after 5-min treatment as shown in Table 1, indicating effective sanitising effect of LcAEW on planktonic cells as the free chlorine content of LcAEW remained within the range of 2–4 mg/L when we covered the container by aluminium foil to avoid volatilisation (Liu et al., 2020). It was worth noting that under the same condition, the survival population of ATCC 35150 remained at around 3.76 log CFU/mL in suspension after LcAEW treatment, which might be due to its higher initial biofilm amount formed on stainless steel coupons (Table 1). Abu-Ali, Ouellette, Henderson, Whittam, and Manning (2010) reported that different strains even in the same *E. coli* O157:H7 lineage could exhibit different gene expression during their colonisation process, leading to different biofilm-forming ability. Another study found that *E. coli* ATCC 25922 could be served as a representative surrogate for

Table 1
Survival of three *E. coli* strains on coupon and in suspension after each 5-min treatment.

	Survival populations on coupon (log CFU/coupon)			Survival populations in suspension (log CFU/mL)		
	ATCC 25922	ATCC 35150	ATCC 43895	ATCC 25922	ATCC 35150	ATCC 43895
Untreatment	7.12 ± 0.15^{a}	7.79 ± 0.10^{a}	7.09 ± 0.24^{a}	ND	ND	ND
DW	6.53 ± 0.04^{b}	7.56 ± 0.11^{ab}	6.47 ± 0.19^{b}	5.81 ± 0.08^{b}	5.57 ± 0.29^{b}	5.64 ± 0.13^{b}
Ultrasound	5.10 ± 0.15^{c}	4.52 ± 0.07^{c}	4.37 ± 0.17^{d}	5.92 ± 0.03^{a}	6.71 ± 0.05^{a}	5.85 ± 0.05^{a}
LcAEW	6.33 ± 0.11^{b}	7.40 ± 0.19^{b}	6.05 ± 0.03^{c}	ND	3.76 ± 0.19^{c}	ND
Combination	ND	3.18 ± 0.17^{d}	ND	ND	ND	ND

Within each column, values with different letters are significantly different ($P < 0.05$). ND: Not detectable: the survival population on coupon <2 log CFU/coupon and the survival population in suspension <2 log CFU/mL.

E. coli O157:H7 due to similar attachment characteristics on food surface (Kim & Harrison, 2009). Our results are consistent with these previous findings showing respective differences and similarities among serotypes and/or strains.

As a comparison, the ultrasound alone treatment resulted in the reduction of three *E. coli* strains by around 2.02–3.27 log CFU/coupon, suggesting that ultrasound could detach the biofilms from coupons effectively through mechanical oscillation. The CLSM images were consistent with the enumeration data, as a significant decrease in cells was observed on coupons, with partly compromised cell membrane structure under cavitation bubble's attack (Fig. S1). However, the population of survival cells in suspension increased after 5 min, which verified again that ultrasound has limited antimicrobial effect but is mainly used for removal purpose (Ishibashi et al., 2010). It was notable that the highest reductions of three *E. coli* strains both on coupons and in suspension were observed after exposure to combined treatment of ultrasound and LcAEW, causing 4.61–6.42 log reductions from coupons and no detectable survival cells in suspension for all strains (Fig. 1 and Table 1). The CLSM results also showed an increase in the proportion of red cells on coupons after this combined treatment, which was quite different from those in control group with much thicker structure (Fig. S1). By collaborating with each other, ultrasound could damage the biofilm structure first and the detached cells from coupons to the suspension were inactivated effectively by LcAEW. However, although this combined method achieved best eradication effect on all *E. coli* biofilms, ATCC 35150 exhibited stronger adhesion ability and removal resistance compared to others, which might be attributed to some differences in its EPS structure and composition. Thus, the overall metabolic profiles of each strain were further evaluated in our study.

3.2. Modelling of antibiofilm effect

The fitting curves of three inactivation models showed similar reduction trends in Fig. 1; however, to determine which one was more suitable to describe the biofilm behaviour under each treatment, the goodness-of-fit of each model is shown in Table S1, as represented by R^2, RMSE and AIC values.

Overall, the modified Weibull model provided the highest R^2 (0.81–0.97), lowest RMSE (0.04–0.71) and AIC (−27.75–8.18) values for all *E. coli* strains after different treatments, demonstrating its universal applicability to describe the inactivation kinetics of *E. coli* biofilms on coupons. When focusing on the combination groups specifically, the reduced Baranyi model was more suitable for describing these groups of data than the modified Weibull model as reflected in its higher R^2 and lower RMSE and AIC values, which was more obvious on the ATCC 35150 strain (Table S1). However, this good appropriateness was reduced in other treatment groups among all strains. The linear model, on the other hand, showed worst fitness by evaluating these parameters, indicating the biofilm removal process induced by these treatments was not linear. These findings were supported by Josewin, Ghate, Kim, and Yuk (2018), who indicated that both the Weibull and Baranyi models could produce a suitable fit for inactivation curves of *Listeria monocytogenes*, which were inoculated on the smoked salmon and treated by the light emitting diode (LED). Comparing the overall results, the modified Weibull model best fitted the data in current study.

To further understand the sensitivity of each *E. coli* biofilm against different treatments, the fitting parameters of the modified Weibull model were determined and are shown in Table 2. The value of the shape parameter, β, was smaller than 1 in all treatment groups among all strains, indicating all inactivation curves displayed downward convexity without inflexion points and shoulders. According to a previous report by Liu et al. (2019), an upwardly survival curve means over the inactivation time, the decline of the population quantity tends to an equilibrium situation. Similarly, the downwardly reduction curve here also indicated the longer the treatment time, the more difficult to detach remaining sturdy cells from coupons. Although the shape parameters did not change regularly among different treatments, the T_R and α values were dependent on the treatment, as the lowest values of them were obtained in the strongest treatment groups (the combined) while the highest values of them were observed in the control groups, which applied to all *E. coli* strains. The minimal T_R values for non-pathogenic *E. coli* and *E. coli* O157:H7 were 0.04 and 0.01 min, respectively, showing ultrasound and LcAEW combination could detach the biofilms from coupons immediately and efficiently. Moreover, additional data (treatment time: 4 min) were used to validate the model performance, which confirmed good predictability of the model with bias percentages smaller than 10% in all treatment groups (data not shown).

Table 2
Fitting parameters of the modified Weibull model for reduction of *E. coli* biofilms from coupons under different treatments.

E. coli strain	Treatment	T_R (min)	α	β
ATCC 25922	DW	38.31 ± 6.02^{a}	2.69 ± 1.13^{a}	0.32 ± 0.07^{a}
	Ultrasound	1.08 ± 0.13^{c}	0.20 ± 0.06^{b}	0.49 ± 0.05^{a}
	LcAEW	12.89 ± 2.26^{b}	1.33 ± 0.76^{ab}	0.39 ± 0.14^{a}
	Combination	0.04 ± 0.00^{c}	0.01 ± 0.00^{b}	0.40 ± 0.00^{a}
ATCC 35150	DW	664.99 ± 81.65^{a}	11.52 ± 3.34^{a}	0.21 ± 0.02^{c}
	Ultrasound	0.06 ± 0.00^{b}	0.00 ± 0.00^{b}	0.35 ± 0.00^{b}
	LcAEW	43.66 ± 9.22^{b}	8.50 ± 1.53^{a}	0.54 ± 0.12^{a}
	Combination	0.01 ± 0.00^{b}	0.00 ± 0.00^{b}	0.21 ± 0.01^{c}
ATCC 43895	DW	358.69 ± 40.32^{a}	0.61 ± 0.51^{a}	0.20 ± 0.10^{a}
	Ultrasound	0.03 ± 0.03^{b}	0.00 ± 0.00^{b}	0.16 ± 0.06^{a}
	LcAEW	22.42 ± 7.73^{b}	0.00 ± 0.00^{b}	0.12 ± 0.03^{a}
	Combination	0.01 ± 0.01^{b}	0.00 ± 0.00^{b}	0.25 ± 0.06^{a}

Note: T_R, time needed for 90% biofilm reduction; α, scale factor; β, shape parameter; DW: deionised water; LcAEW: low concentration acidic electrolysed water; Combination: ultrasound + LcAEW; Different letters represent significantly differences among different treatments within each strain ($P < 0.05$).

Mathematical models can help us predict the inactivation effect through statistical analysis. In previous studies, the Weibull model also proved the most suitable model for describing antimicrobial effects of nisin and grape seed extract against L. *monocytogenes* on shrimps, with good consistency between predicted and observed values (Zhao, Chen, Zhao, He, & Yang, 2020). Moreover, Ghate et al. (2017) found that the Weibull model could fit well the inactivation kinetics of *Salmonella* on fresh-cut pineapples under LED illumination, with its unique compatibility with the biphasic characteristic of LED's antimicrobial effect. In addition to providing relatively accurate quantifications, model fitting could also be used as a tool for comparing antimicrobial kinetics under different conditions, providing detailed information about sensitivity and resistance of microorganisms against different treatments during inactivation process.

3.3. Metabolite profiling of E. coli biofilms after treatments

The typical ^{1}H NMR spectra of three *E. coli* biofilms after each treatment are shown in Fig. S2. In total, 50 metabolites were identified and their detailed resonance assignments are shown in Table S2. The two strains of *E. coli* O157:H7 displayed high similarity in their metabolite variety, with 19 amino acids, 9 organic acids, 7 sugars, 7 nucleotide-related compounds and 8 other metabolites observed in the region of 0.5–9.5 ppm. Different intensity and diversity of some metabolite signals were found in the non-pathogenic *E. coli* spectra. For instance, the intensities of ^{1}H resonance at 2.21, 5.12 and 8.84 ppm, which was assigned as acetoin, phosphoenolpyruvic acid (PEP) and nicotinamide adenine dinucleotide (NAD), respectively, were stronger in ATCC 25922 than those in other two counterparts (Fig. S2).

One previous study suggested that substantial metabolic differences could exist in *E. coli* strains even they are closely related phylogenetically (Van Der Hooft, Goldstone, Harris, Burgess, & Smith, 2019). On the other hand, Hancock, Vejborg, and Klemm (2010) found the distance between pathogenic and non-pathogenic *E. coli* strains sometimes could be very short, as they might be distinguished by just a few hundred

genes. These seeming conflicting opinions might be derived from different studied strains. In this study, serovar-specific metabolic traits were observed among three *E. coli* biofilms, along with sharing many kinds of metabolites in common.

Furthermore, to identify the metabolite level changes in each *E. coli* biofilm under the stresses, a heat map of 32 metabolites with no overlapping chemical shifts was plotted for relative quantification (Fig. S3). Based on the z-score values, the deeper green and red colour represent lower and higher level of metabolites, respectively. In ATCC 25922, the levels of most amino acids (*e.g.,* Leu, Val, Thr, Arg) were increased after single ultrasound treatment, showing opposite trends compared to their changes in planktonic cells as observed in our previous research (Zhao, Zhao, Wu, et al., 2019), and indicating biofilm-associated resistance and survival strategy to ultrasound stress. However, when combined with LcAEW, a marked depletion of most amino acids and nucleotide-related compounds as well as all organic acids and sugars was observed. This was like the metabolite changes in planktonic cells after same combined treatment, indicating mature non-pathogenic *E. coli* biofilm failed to produce effective adaptive responses when facing excessive stresses and shared many similarities in the stress response with bacteria in stationary growth phase (Beloin et al., 2004). Whereas in the *E. coli* O157:H7 strains, the levels of most metabolites showed a trend of fluctuation compared with their respective control groups after the combined treatment. Álvarez-Ordóñez et al. (2013) found that the *E. coli* strains belonging to the serogroup O157 exhibited more tolerance to environmental stresses (*e.g.,* acid, heat and high pressure), while the non-pathogenic strains tended to be most sensitive. Our results were in accordance with these findings, as *E. coli* O157:H7 biofilms we studied here showed some efforts for maintaining the levels of a series of metabolites to improve resistance. Therefore, to further investigate which metabolites played important roles in modulating the stress response, following analyses were carried out by screening the principal metabolites.

3.4. Principal components analysis

The model quality parameters, R^2X and Q^2 shown in Fig. 2A1–C1, were used to evaluate PCA model's interpretative and predictable abilities, respectively. For *E. coli* O157:H7 strains, the first three PCs of ATCC 35150 and ATCC 43895 explained 97.0% (PC1: 63.9%; PC2: 22.2%; PC3: 10.9%) and 97.8% (PC1: 64.8%; PC2: 24.2%; PC3: 8.8%) of the total data, respectively, whereas in the non-pathogenic strain, PC1, PC2 and PC3 explained 60.7%, 18.1% and 9.6%, respectively, showing the fitness of the model might be compromised relatively. Moreover, the

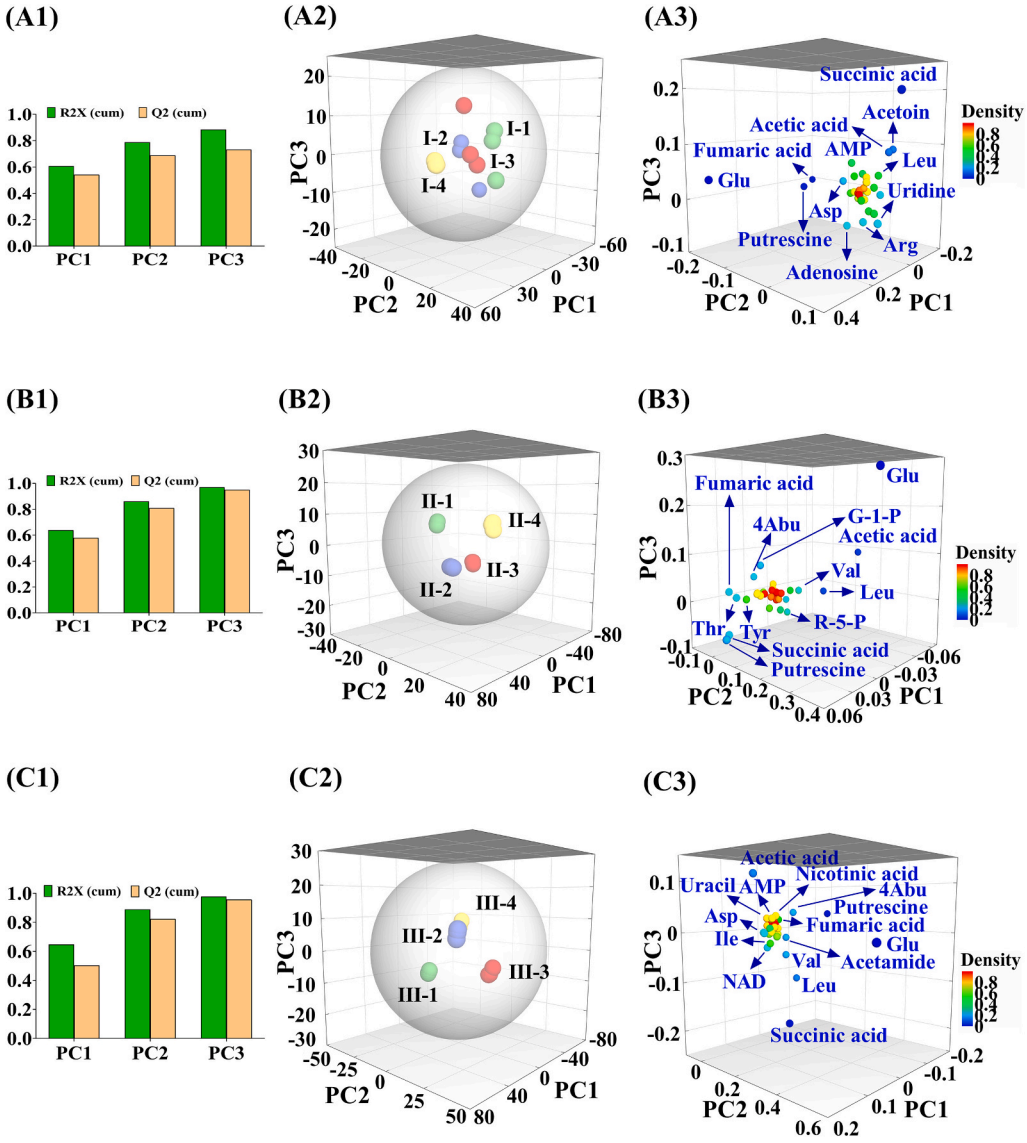

Fig. 2. Principal component analysis (PCA) of three *E. coli* strains under different treatments. A1, B1, C1: The principal components explaining variances used in the PCA models; A2, B2, C2: the 3D score plot of PCA; A3, B3, C3: The 3D loading plot of PCA. Note: R^2X: explained variable value; Q^2: model predictability value; I: ATCC 25922; II: ATCC 35150; III: ATCC 43895; 1: deionised water (DW) treatment; 2: ultrasound treatment; 3: low concentration acidic electrolysed water (LcAEW) treatment; 4: combination of ultrasound and LcAEW treatment.

Q^2 values of three strains lied within the range of 0.73–0.96, which were more than 0.5 indicating good model predictability (Wiklund, 2008).

The samples of each strain after different treatments were well separated into several clusters, as shown in the score plots (Fig. 2A2–C2). The most distinctive separation of ATCC 25922 was observed between the control and combined group, suggesting the synergic stress of ultrasound and LcAEW could cause the largest changes of metabolites. However, in *E. coli* O157:H7 strains, the samples after being treated by LcAEW alone or combined with ultrasound showed similar distances from their respective control group, by calculating the given score variables shown in Table S3. Moreover, the relative squared cosines of the three PCs characterising each group are displayed in Table S4, which could help us find which component played a more significant role in interpreting the variables (Abdi & Williams, 2010). For example, ultrasound alone and combined with LcAEW groups in ATCC 25922, single ultrasound and LcAEW groups in ATCC 35150, and all four groups in ATCC 43895 were affected mainly by PC1, while other groups were influenced more by other two PCs.

Moreover, the discriminative metabolites that contributed to these group separations of each strain are presented respectively in the loading plots (Fig. 2A3–C3). In ATCC 25922, Glu, acetoin, fumaric acid, acetic acid and succinic acid were mainly characterised by PC1 and PC2, PC1 and PC3, PC1 and PC2, PC1 and PC3, PC2 and PC3, respectively. Similar metabolites with distinctive loadings on the three PCs were observed in *E. coli* O157:H7 strains, along with some strain-specific metabolites (*e.g.,* γ-aminobutyric acid (4Abu)) as shown in Table S5. These metabolites could be recognised as potential biomarkers that responded to different treatments by comparing their cos^2 values (Table S6) with those of score variables in Table S5. For instance, Val, Glu, β-D-glucose, glucose-6-phosphate and PEP might be closely related to the groups containing ultrasound in ATCC 25922, while the combined group of ATCC 35150 could be characterised by Asp, UMP and acetamide specifically. The results suggested that *E. coli* biofilms exhibited a diversity of metabolic responses under stresses, making their different removal kinetics from coupons reasonable.

3.5. Alternative metabolites during the combined treatment

To further study the metabolic response of *E. coli* biofilms following the combined treatment of ultrasound and LcAEW, OPLS-DA was conducted to visualise separations between the control and combined groups. As shown in the left sides of Fig. 3A–C, all pairwise comparisons

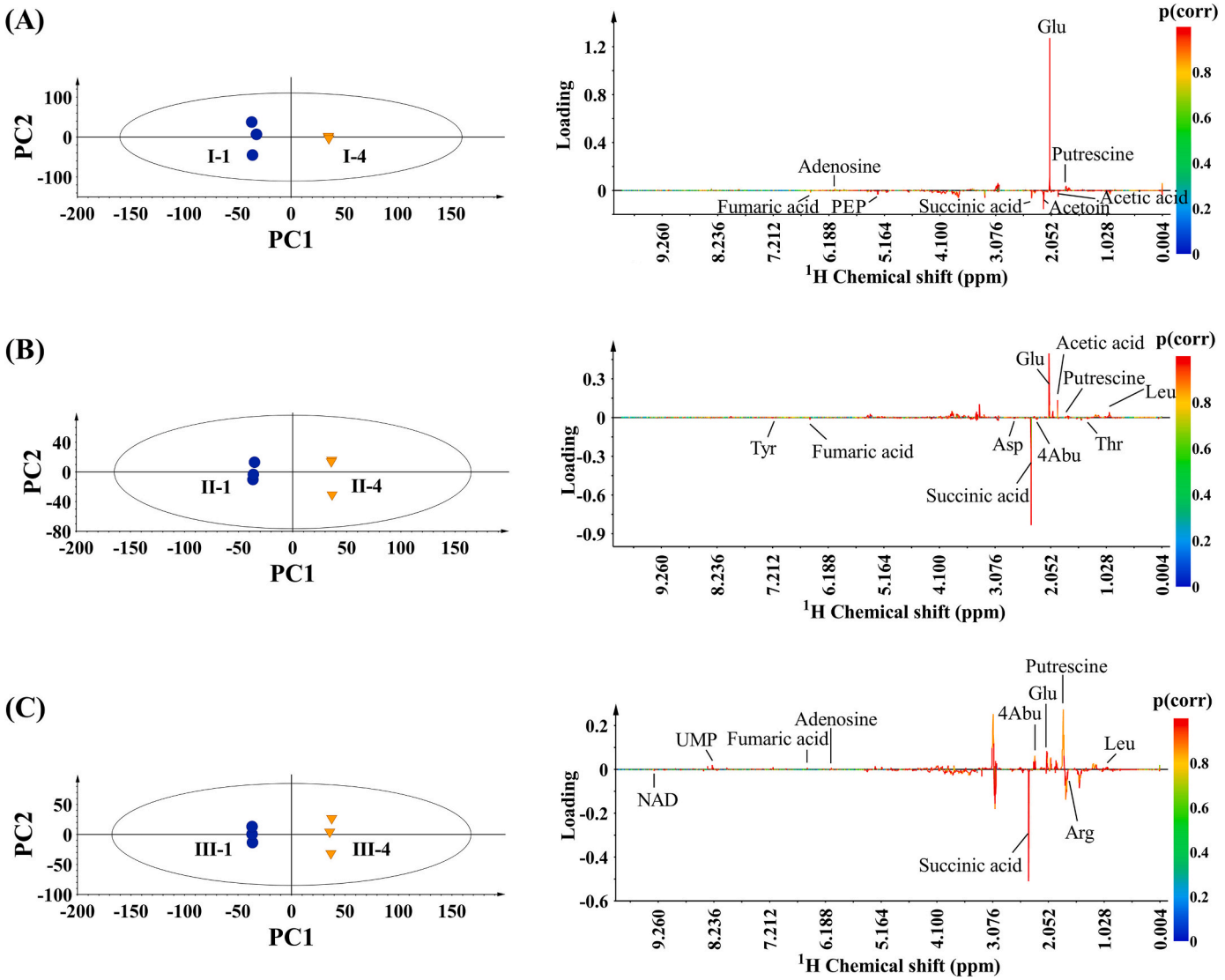

Fig. 3. Orthogonal projection to latent structure discriminant analysis (OPLS-DA) score plots (left side of A, B, C) and coefficient-coded loading S-lines (right side of A, B, C) for the control and combined treatment groups. I: ATCC 25922; II: ATCC 35150; III: ATCC 43895; 1: DW treatment; 4: combination of ultrasound and LcAEW treatment.

demonstrated clear separations with good model fitness and predictability (ATCC 25922: $R^2X = 0.874$, $Q^2 = 0.990$; ATCC 35150: $R^2X = 0.764$, $Q^2 = 0.985$; ATCC 43895: $R^2X = 0.818$, $Q^2 = 0.992$). The loading S-line in the right side showed major metabolites that resulted in these pairwise differentiations, with downward and upward peaks illustrating lower and higher levels of metabolites in the combined group compared to those in the control group, respectively. In ATCC 25922, except Arg, Glu, Asp, uridine, adenosine, putrescine and NAD, decreased contents of other metabolites were detected in the combined group. For *E. coli* O157:H7 strains, higher concentration of around half of metabolites was associated with the combined stimulation.

Moreover, volcano plot of each strain was generated based on the metabolite's correlation coefficient, VIP, FC, and *P* values, as shown in Fig. 4A1–C1. Metabolites with a FC > 1.5 and $P < 0.05$ were considered as statistically significant (Wu et al., 2021). In ATCC 25922, acetic acid, α-D-glucose, uracil and G-1-P coloured in blue were located in the negative side of the x-axis, indicating these metabolites were most susceptible to the combined treatment compared to other reduced counterparts. On the other hand, Glu was most closely related to the combined stress among the seven increased metabolites as mentioned above. The metabolites significantly influenced by the combined treatment were different in *E. coli* O157:H7 strains, as Glu, acetic acid, Leu,

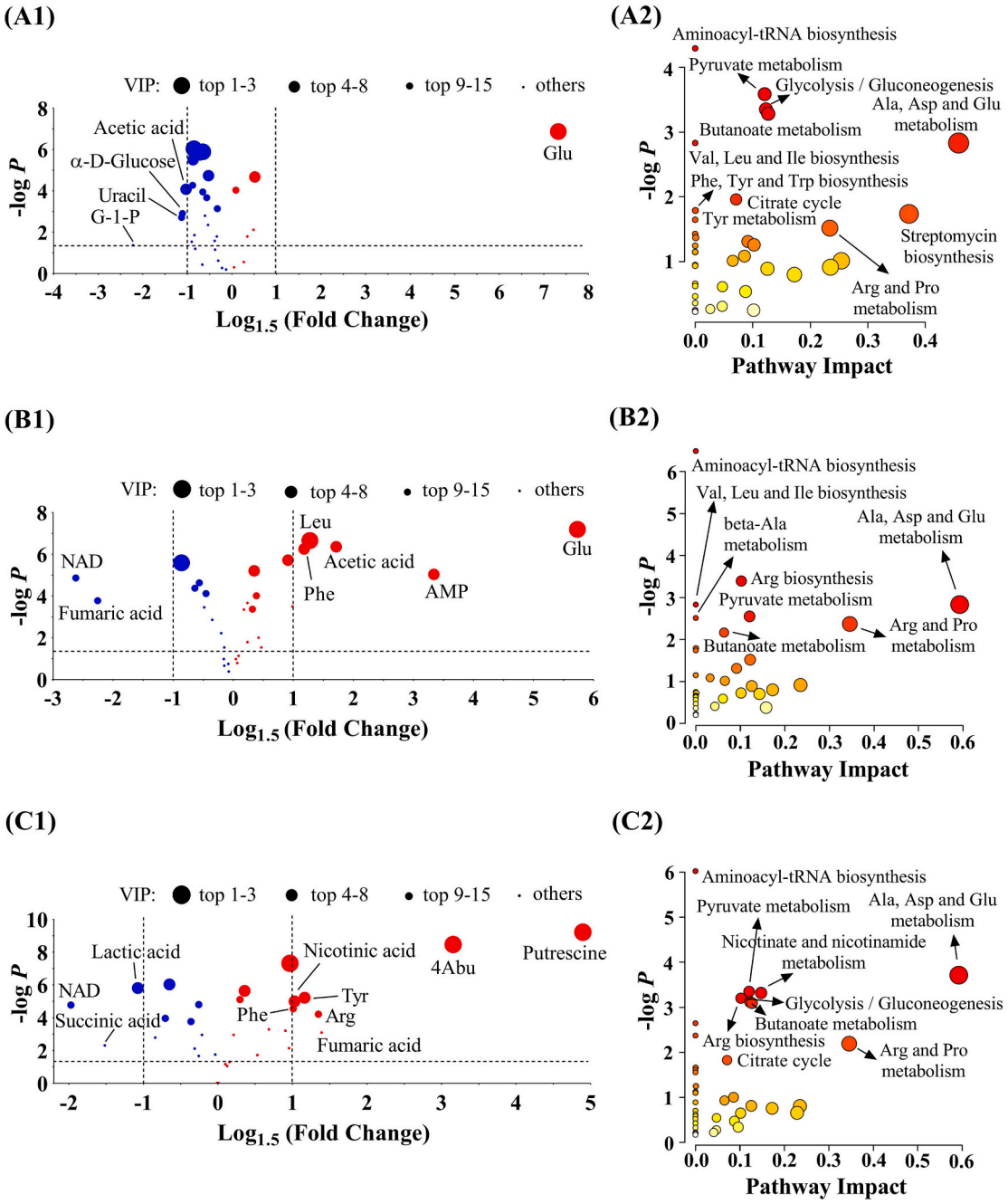

Fig. 4. Volcano plot of screened *E. coli* metabolites in control and combined treatment groups (A1-C1) and overview of pathway analysis of control and combined treatment groups (A2-C2). Note: A: ATCC 25922; B: ATCC 35150; C: ATCC 43895. For volcano plot, metabolites coloured in red or blue represent higher or lower content in combined group as compared to the control group, respectively. For pathway analysis, each circle represents one pathway, and the colour and size of each circle is based on the *P* value and the pathway impact value, respectively. (For interpretation of the references to colour in this figure legend, the reader is referred to the web version of this article.)

Phe and AMP were highlighted with significant increases in ATCC 35150 whereas this significantly increasing trend happened to putrescine, 4Abu, nicotinic acid, fumaric acid, Arg and Tyr in ATCC 43895. These statistically significant metabolites can be seen as potential biomarkers to characterise injured cells during this combined stress.

A schematic model illustrating the antibiofilm mechanism of ultrasound and LcAEW from multiple attacking targets is proposed in Fig. 5. Composition of EPS is complex and may vary between different strains of *E. coli*, but in general, polysaccharides are prominent components in EPS that provide structural support for the biofilm, accompanied by other substances such as proteins, lipids and extracellular DNA (eDNA) (Koo, Allan, Howlin, Stoodley, & Hall-Stoodley, 2017). These biomolecules in EPS can get hit first under external treatments.

Previous studies showed that the antibiofilm mechanism by ultrasonic waves was mainly attributed to their cavitation effect, which can destroy EPS structure through the implosive collapse of cavitating bubbles with the help of shock waves and microstreaming (Vyas et al., 2019). This mechanical oscillation could destroy polysaccharides in the EPS by breaking their glycosidic bonds, making increased content of glucose in ATCC 25922 and ATCC 43895 reasonable after ultrasound treatment (Nachtigall et al., 2019). However, the opposite trend observed in ATCC 35150 might be due to its different polysaccharide structure, as polysaccharide with longer side chain might exhibit less sensitivity to external stress (Nachtigall, Rohm, & Jaros, 2021). Besides mechanical oscillation, free radicals (*e.g.,* H· and ·OH) and strong oxides (*e.g.,* H_2O_2) generated by the hydrolysis of water during cavities' implosion also played an important role in damaging EPS components. For example, some specific amino acid residues on extracellular proteins might be attacked and inactivated by the generated oxides, which could explain why most amino acid levels (Iso, Leu, Val, Thr, etc.) in *E. coli* O157:H7 strains were decreased under ultrasound stress (Yu et al., 2020). On the other hand, the channels that transport nutrients and oxygen to the deeper layers of the biofilm could be activated by ultrasound, stimulating bacterial metabolism from starved state and supporting biosynthesis of some components in the EPS, which might be an explanation for increased levels of some amino acids in ATCC 25922 (Erriu et al., 2014).

The interaction between LcAEW and macromolecules in EPS could change EPS content and composition as well. For example, Han et al. (2017) found that after AEW treatment on *E. coli* biofilms, the C-O-C bonds of polysaccharides in the EPS and the aromatic rings in tyrosine and phenylalanine of EPS protein were deformed, accompanied by the destruction of the ring structure of the eDNA. Similar results were observed in our study, as the decreased levels of most carbohydrates and nucleotide-related compounds occurred in all *E. coli* biofilms after LcAEW treatment. It has been believed that the eradication effect of LcAEW on biofilm could be attributed to its chlorination and oxidation properties, as its chlorine compounds (*e.g.,* HOCl, $^{-}$OCl) and free radicals (*e.g.,* ·OH) could react simultaneously with the macromolecules in EPS (Sam & Lu, 2009). However, these reactions could decrease chlorine availability of LcAEW and lead to a compromised antimicrobial effect on inner biofilm cells. This dilemma could be solved by combining LcAEW with ultrasound, as the latter could damage the EPS matrix and make inner cells scattered and exposed to the former, achieving a synergistic antibiofilm effect. Moreover, at the cellular level, the cavitation bubbles produced by ultrasound could damage cell exteriors, which benefits the penetration of LcAEW into the cells, and in turn, the injured cells could be further disintegrated by ultrasound (Li et al., 2017). Under this combined stress, the normal metabolic activities inside bacterial cells could be disrupted or suppressed, inducing cell necrosis and apoptosis.

Generally, the bactericidal effect of ultrasound can be mainly attributed to two factors: (1) mechanical oscillation, which can alter cell wall structure and membrane permeability; (2) collapse cavitation, which can generate high pressure and temperature, induce shear forces, and form reactive oxygen species (ROS) during the collapse of gas bubbles (Erriu et al., 2014). For LcAEW, the chlorine compounds (HOCl, $^{-}$OCl, Cl_2), pH, ORP, and ROS (OH^{-}, O^{-}) can affect its antimicrobial efficacy together (He, Zhao, Chen, Zhao, & Yang, 2021; Zhao, Li, & Yang, 2021). When these physical and chemical stresses acted on the *E. coli* cells as a combination, normal cellular ultrastructure and metabolic profiles could be changed as shown in the upper part of Fig. 5. The ROS accumulation in bacteria can oxidise functional molecules that contain reactive residues (*e.g.,* peptide bonds, thiol groups and amino groups), causing a series of metabolite changes such as protein synthesis inhibition and DNA oxidation (Liao et al., 2018). On the other hand, a perturbation of energy metabolism also happened during this combined treatment, with decreased levels of ADP observed in all *E. coli* strains. Considering the high ORP of LcAEW might influence the ATP production and the produced ATP could be lost due to broken cell membrane, it was very likely that the energy supply cannot meet the increased bacterial demand for energy in response to the stresses, causing a depressed growth pattern (Colangelo et al., 2015). Additionally, the normal functions of ion channels on the cell membrane could be damaged by mechanical force and/or conductivity change under this combined treatment, resulting in the influx of Na^{+} and Ca^{2+} and the outflux of K^{+}, protein and DNA, which could induce osmotic imbalance and disturb intracellular metabolic flux in further (Zeng et al., 2010).

3.6. Pathway analysis

To comprehensively study the metabolic network activity under ultrasound and LcAEW stresses, associated pathway analysis was carried out based on the selected metabolites with VIP value >1. As shown in Fig. 4A2–C2, a total of 40, 36 and 44 pathways were involved for ATCC 25922, ATCC 35150 and ATCC 43895, respectively, among which 15, 13 and 15 pathways with $P < 0.05$ were significantly affected in each as shown in Table S7. The main affected pathways of three *E. coli* strains under ultrasound, LcAEW and their combination treatments are summarised and sketched in Fig. 6, including amino acid metabolism, nucleotide metabolism, energy metabolism and carbohydrate metabolism.

Multiple stresses (*e.g.,* oxidative, acidic pH, osmotic and heat stresses) brought by ultrasound and LcAEW treatments can have a cross-impact on *E. coli* pathway alterations, while simultaneously, *E. coli* biofilms can activate multiple regulators as adaptive responses toward these stresses, and usually the induction of one regulator due to one particular stress tends to show cross-protection against other stresses concurrently (Fernández et al., 2018). The up- and down-regulation of some genes might be responsible for the increased resistance of biofilms to sanitisers compared to their planktonic counterparts.

It has been reported that HOCl can activate *soxRS* and *oxyR* expression in *E. coli* to produce SoxR, SoxS and OxyR protein, which can act as antioxidant systems and protect the cell from attack of superoxide anion and hydrogen peroxide, respectively (Lushchak, 2011). Therefore, the elevated levels of some amino acids like Iso, Leu and Val in ATCC 35150 biofilm after treatments containing LcAEW might imply some strain-specific protein biosynthesis responses as its adaptation to oxidative stress, indicating its better adaptive ability during oxidative challenge than the other two strains and making its only survival in suspension reasonable as shown in Table 1. However, aromatic and sulfurous amino acids such as Phe, Tyr, Met and Cys were reported to be more sensitive to oxidative stress (Yang et al., 2019), which might cause corresponding effect on the content of their precursors and products.

On the other hand, glutamate decarboxylase (GAD) system can be upregulated in acidic condition and help remove intracellular protons by converting Glu to 4Abu through decarboxylation reaction. As many oxidative reactions are affected by the pH, this GAD acid-resistance system can also provide oxidative stress protection by maintaining intracellular pH homoeostasis (Chen et al., 2022). However, the higher contents of Glu in all treated *E. coli* strains in our study indicated that the conversion rate of Glu to 4Abu was low. Bearson, Lee, and Casey (2009) demonstrated that the induction of GAD activity required low pH such as

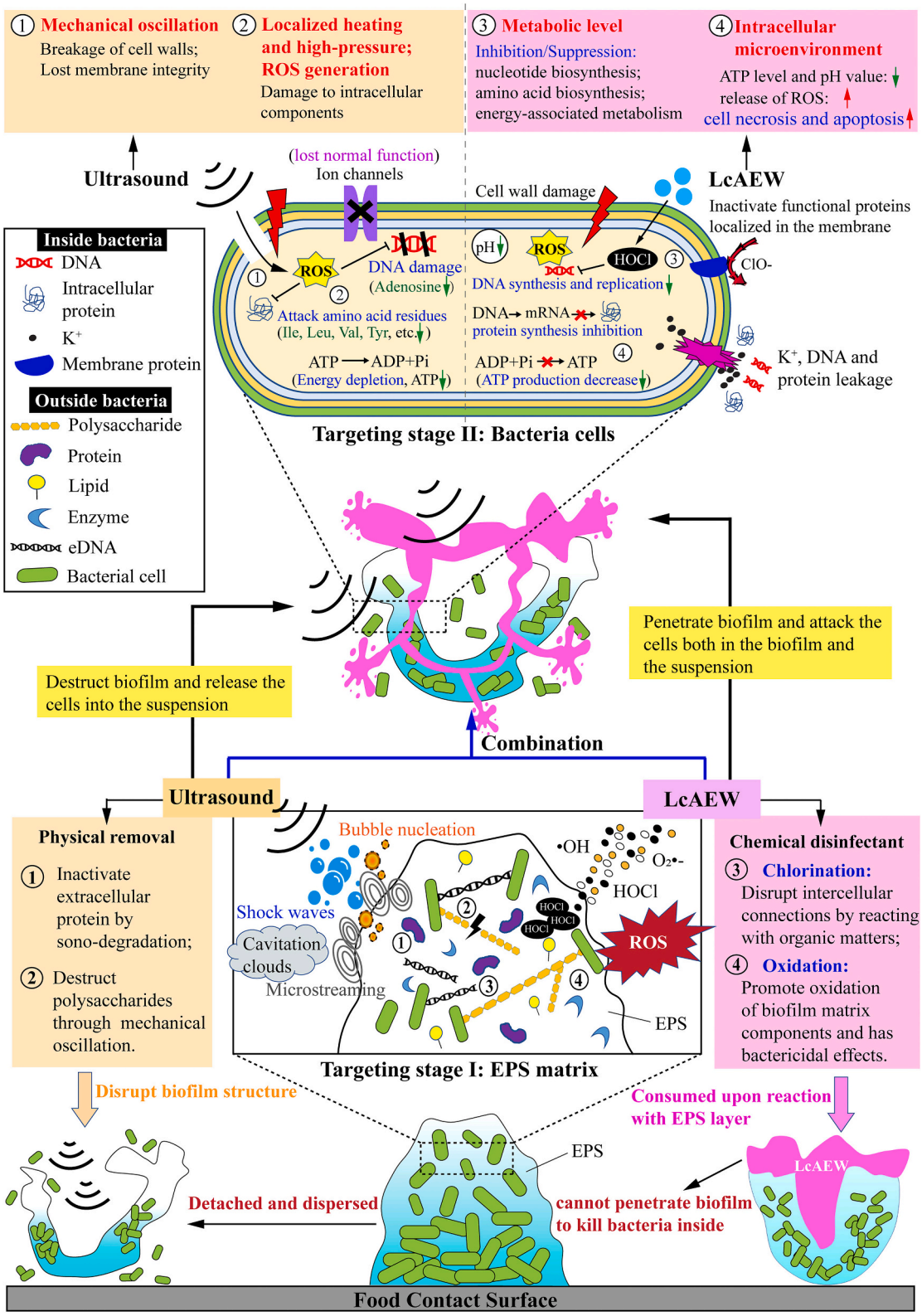

Fig. 5. Hypothetical target sites and mechanisms of action of ultrasound and LcAEW on *E. coli* biofilm. The extracellular polymeric substances (EPS) structure and macromolecules (*e.g.*, extracellular protein, polysaccharide, eDNA) within mature biofilms established on the food contact surface can be disrupted and degraded by ultrasound and LcAEW, which can be regarded as first targeting stage of the treatments. Under the combination, the biofilm structure is damaged and the cells in the deep layers of biofilm are exposed and attacked, experiencing a series of intracellular metabolite changes.

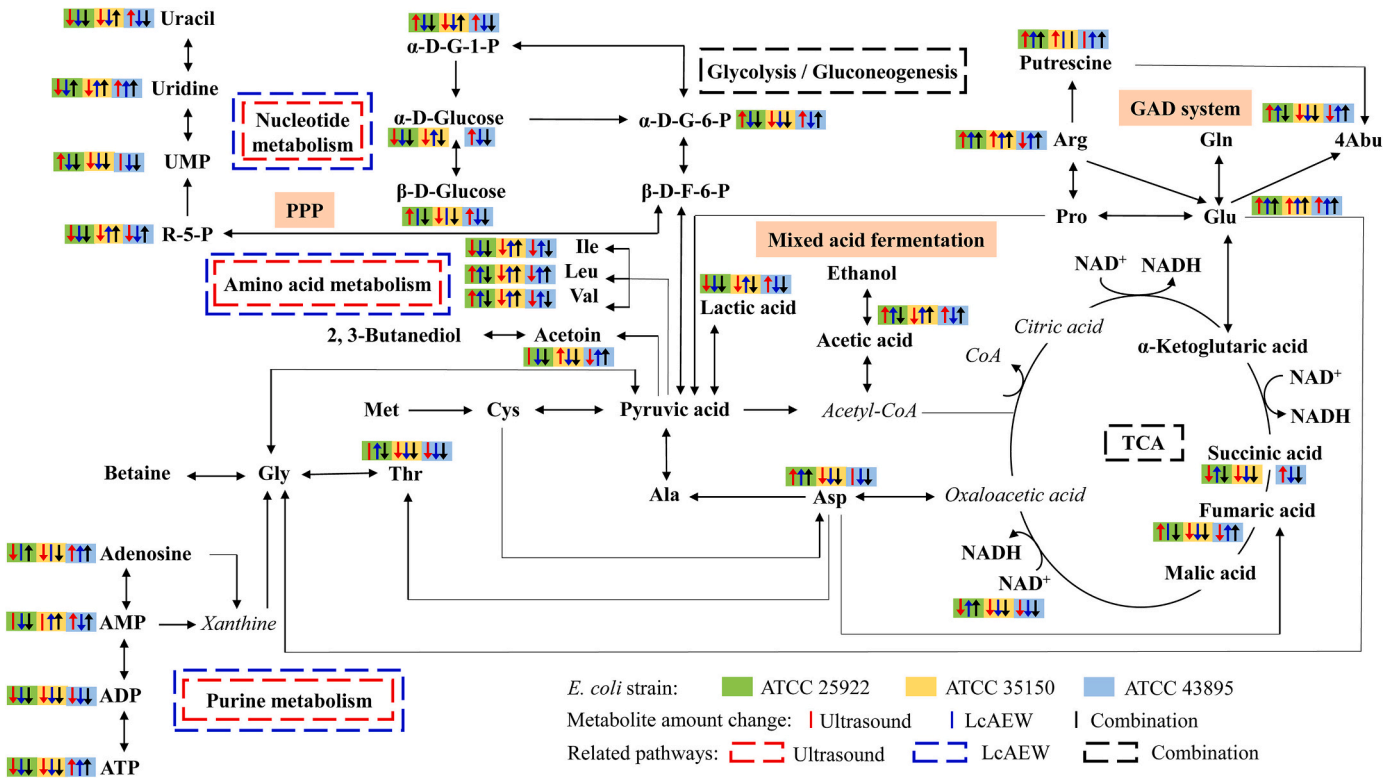

Fig. 6. Proposed schematic of metabolic alterations upon ultrasound, LcAEW and their combined treatment on three *E. coli* strains. Note: upward and downward arrows beside quantified metabolites indicate higher and lower concentration in ATCC 25922 (green shadow), ATCC 35150 (yellow shadow) and ATCC 43895 (blue shadow) after ultrasound (red line), LcAEW (blue line) and their combined (black line) treatments, respectively. No arrow means unchanged amount. The main pathways affected by ultrasound, LcAEW and their combined treatment are framed in red, blue and black boxes, respectively. (For interpretation of the references to colour in this figure legend, the reader is referred to the web version of this article.)

2.5, so the pH 4.0 of LcAEW used in this study might situate GAD in a non-optimal status for providing sufficient protection against acidic and oxidative stresses. Moreover, some amino acids (*e.g.,* Pro, Val) can act as osmoprotectants to maintain the stabilisation of cytoplasm osmolality when faced with osmotic stress, which could also be one possible reason for increased levels of some amino acids (*e.g.,* Arg, Val) under the combined treatment (O'Byrne & Booth, 2002; Valle et al., 2008).

However, the multiple stress-response regulators can only partially compensate the impaired pathways when microbes face compounding and excessive stresses. In this study, lower content of glucose and higher content of PEP (an intermediate can be converted to pyruvic acid) indicated an unbalanced glycolysis of *E. coli* strains under combined treatment, which in further repressed tricarboxylic acid (TCA) cycle as many TCA cycle related metabolite levels (*e.g.,* succinic acid, fumaric acid and NAD) were decreased. Koebmann, Westerhoff, Snoep, Nilsson, and Jensen (2002) demonstrated glycolysis in *E. coli* can be controlled in an ATP-dependent manner, in which increased ATP hydrolysis and lower ATP/ADP ratio could result in an increased glycolytic flux. Therefore, the reduction of ATP level mentioned in Section 3.5 could induce more glucose consumption in stressed cells, especially in ATCC 25922 and ATCC 35150, while an increase of ATP level in ATCC 43895 might imply an energy conservation strategy for survival. On the other hand, as a central metabolic pathway providing many precursors and intermediates for other processes, the disturbance of TCA cycle could make many related metabolic networks affected (Zhang et al., 2018), such as Ala- and Asp-dependent protein metabolism and α-ketoglutaric acid-associated Glu metabolism, which were subject to various degree changes in our study.

As alternative shunts for sustaining glycolysis concomitantly, the pentose phosphate pathway (PPP) and the mixed acid fermentation could also be affected under stresses (Bertels, Fernández Murillo, & Heinisch, 2021; Vidra & Németh, 2018), with depleted level of ribose-5-phosphate (R-5-P) and increased level of acetic acid observed more apparently in ATCC 25922 than in the pathogenic strains in our study. Considering R-5-P is an important precursor for nucleotide biosynthesis, its diminishment indicated impaired DNA replication and cell proliferation. Moreover, the metabolic switch from oxidation to mixed acid fermentation producing lactic acid, acetic acid and ethanol could be recognised as an adaptive strategy of bacteria, when they were situated in a low oxygen environment under LcAEW and ultrasound treatments (Schalenbach, Zeradjanin, Kasian, Cherevko, & Mayrhofer, 2018).

4. Conclusion

The antibiofilm effects and mechanisms of ultrasound and LcAEW combination against different *E. coli* strains were investigated. Specifically, ultrasound mainly damaged the EPS and cell wall structure by mechanical oscillation, whereas LcAEW attacked intracellular metabolic flux as a leading antimicrobial mechanism. This study suggested that NMR-based metabolomics strategy could be used to explain antibiofilm mechanisms of disinfection interventions on biofilm removal process, providing guidance for further mechanism research related to food contact surface sanitisation. Meanwhile, the combination of ultrasound and LcAEW is worthy of utilisation as an effective biofilm control measure in food processing plants where biofilms are a problem on food contact surface, especially in organic food industry.

Declaration of interests

The authors declare that they have no known competing financial interests or personal relationships that could have appeared to influence the work reported in this paper.

Acknowledgements

This study was funded by Applied Basic Research Project (Agricultural) Suzhou Science and Technology Planning Programme (SNG2020061), Natural Science Foundation of Jiangsu Province (BK20181184), Singapore Ministry of Education Academic Research Fund Tier 1 (R-160-000-A40-114), and an industry grant supported by Shenzhen Zhiyun Optoelectronics Co., Ltd. (R-143-000-A24-597).

Appendix A. Supplementary data

Supplementary data to this article can be found online at https://doi.org/10.1016/j.ifset.2022.102917.

References

Abdi, H., & Williams, L. J. (2010). Principal component analysis. *Wiley Interdisciplinary Reviews: Computational Statistics, 2*(4), 433–459.

Abu-Ali, G. S., Ouellette, L. M., Henderson, S. T., Whittam, T. S., & Manning, S. D. (2010). Differences in adherence and virulence gene expression between two outbreak strains of enterohaemorrhagic *Escherichia coli* O157:H7. *Microbiology, 156*(Pt 2), 408.

Adhikari, A., Syamaladevi, R. M., Killinger, K., & Sablani, S. S. (2015). Ultraviolet-C light inactivation of *Escherichia coli* O157:H7 and *Listeria monocytogenes* on organic fruit surfaces. *International Journal of Food Microbiology, 210*, 136–142.

Álvarez-Ordóñez, A., Alvseike, O., Omer, M., Heir, E., Axelsson, L., Holck, A., & Prieto, M. (2013). Heterogeneity in resistance to food-related stresses and biofilm formation ability among verocytotoxigenic *Escherichia coli* strains. *International Journal of Food Microbiology, 161*(3), 220–230.

Ayebah, B., Hung, Y. C., Kim, C., & Frank, J. F. (2006). Efficacy of electrolyzed water in the inactivation of planktonic and biofilm *Listeria monocytogenes* in the presence of organic matter. *Journal of Food Protection, 69*(9), 2143–2150.

Bang, H.-J., Park, S. Y., Kim, S. E., Rahaman, M. M. F., & Ha, S.-D. (2017). Synergistic effects of combined ultrasound and peroxyacetic acid treatments against *Cronobacter sakazakii* biofilms on fresh cucumber. *LWT, 84*, 91–98.

Baranyi, J., & Roberts, T. A. (1995). Mathematics of predictive food microbiology. *International Journal of Food Microbiology, 26*(2), 199–218.

Bearson, B. L., Lee, I. S., & Casey, T. A. (2009). *Escherichia coli* O157:H7 glutamate-and arginine-dependent acid-resistance systems protect against oxidative stress during extreme acid challenge. *Microbiology, 155*(3), 805–812.

Beloin, C., Valle, J., Latour-Lambert, P., Faure, P., Kzreminski, M., Balestrino, D., … Ghigo, J. M. (2004). Global impact of mature biofilm lifestyle on *Escherichia coli* K-12 gene expression. *Molecular Microbiology, 51*(3), 659–674.

Berrang, M. E., Frank, J. F., & Meinersmann, R. J. (2008). Effect of chemical sanitizers with and without ultrasonication on *Listeria monocytogenes* as a biofilm within polyvinyl chloride drain pipes. *Journal of Food Protection, 71*(1), 66–69.

Bertels, L.-K., Fernández Murillo, L., & Heinisch, J. J. (2021). The pentose phosphate pathway in yeasts–more than a poor cousin of glycolysis. *Biomolecules, 11*(5), 725.

Chen, G. W., Chen, Y. A., Chang, H. Y., Huang, T. C., & Chen, T. Y. (2021). Combined impact of high-pressure processing and slightly acidic electrolysed water on *Listeria monocytogenes* proteomes. *Food Research International, 147*, Article 110494.

Chen, L., Liu, Q., Zhao, X., Zhang, H., Pang, X., & Yang, H. (2022). Inactivation efficacies of lactic acid and mild heat treatments against *Escherichia coli* strains in organic broccoli sprouts. *Food Control, 133*, Article 108577.

Colangelo, M. A., Caruso, M. C., Favati, F., Scarpa, T., Condelli, N., & Galgano, F. (2015). Electrolysed water in the food industry as supporting of environmental sustainability. In A. Vastola (Ed.), *The Sustainability of Agro-Food and Natural Resource Systems in the Mediterranean Basin* (pp. 385–397).

Cui, H., Li, H., Abdel-Samie, M. A., Surendhiran, D., & Lin, L. (2021). Anti-*Listeria monocytogenes* biofilm mechanism of cold nitrogen plasma. *Innovative Food Science & Emerging Technologies, 67*, Article 102571.

Ding, T., Ge, Z., Shi, J., Xu, Y. T., Jones, C. L., & Liu, D. H. (2015). Impact of slightly acidic electrolyzed water (SAEW) and ultrasound on microbial loads and quality of fresh fruits. *LWT, 60*(2), 1195–1199.

Erriu, M., Blus, C., Szmukler-Moncler, S., Buogo, S., Levi, R., Barbato, G., Madonnaripa, D., Denotti, G., Piras, V., & Orrù, G. (2014). Microbial biofilm modulation by ultrasound: current concepts and controversies. *Ultrasonics Sonochemistry, 21*(1), 15–22.

Fernández, A., Cebrián, G., Álvarez-Ordóñez, A., Prieto, M., Bernardo, A., & López, M. (2018). Influence of acid and low-temperature adaptation on pulsed electric fields resistance of *Enterococcus faecium* in media of different pH. *Innovative Food Science & Emerging Technologies, 45*, 382–389.

Gao, S., Lewis, G. D., Ashokkumar, M., & Hemar, Y. (2014). Inactivation of microorganisms by low-frequency high-power ultrasound: 1. Effect of growth phase and capsule properties of the bacteria. *Ultrasonics Sonochemistry, 21*(1), 446–453.

Ghate, V., Kumar, A., Kim, M.-J., Bang, W.-S., Zhou, W., & Yuk, H.-G. (2017). Effect of 460 nm light emitting diode illumination on survival of *Salmonella* spp. on fresh-cut pineapples at different irradiances and temperatures. *Journal of Food Engineering, 196*, 130–138.

Hamilton, S., Bongaerts, R. J., Mulholland, F., Cochrane, B., Porter, J., Lucchini, S., … Hinton, J. C. (2009). The transcriptional programme of *Salmonella enterica* serovar Typhimurium reveals a key role for tryptophan metabolism in biofilms. *BMC Genomics, 10*(1), 1–21.

Han, Q., Song, X., Zhang, Z., Fu, J., Wang, X., Malakar, P. K., … Zhao, Y. (2017). Removal of foodborne pathogen biofilms by acidic electrolyzed water. *Frontiers in Microbiology, 8*, 988.

Hancock, V., Vejborg, R. M., & Klemm, P. (2010). Functional genomics of probiotic *Escherichia coli* Nissle 1917 and 83972, and UPEC strain CFT073: comparison of transcriptomes, growth and biofilm formation. *Molecular Genetics and Genomics, 284*(6), 437–454.

He, Y., Zhao, X., Chen, L., Zhao, L., & Yang, H. (2021). Effect of electrolysed water generated by sodium chloride combined with sodium bicarbonate solution against *Listeria innocua* in broth and on shrimp. *Food Control, 127*, Article 108134.

Huang, L. (2009). Thermal inactivation of *Listeria monocytogenes* in ground beef under isothermal and dynamic temperature conditions. *Journal of Food Engineering, 90*(3), 380–387.

Ishibashi, K., Shimada, K., Kawato, T., Kaji, S., Maeno, M., Sato, S., & Ito, K. (2010). Inhibitory effects of low-energy pulsed ultrasonic stimulation on cell surface protein antigen C through heat shock proteins GroEL and DnaK in *Streptococcus mutans*. *Applied and Environmental Microbiology, 76*(3), 751–756.

Jamal, M., Ahmad, W., Andleeb, S., Jalil, F., Imran, M., Nawaz, M. A., … Kamil, M. A. (2018). Bacterial biofilm and associated infections. *Journal of the Chinese Medical Association, 81*(1), 7–11.

Josewin, S. W., Ghate, V., Kim, M.-J., & Yuk, H.-G. (2018). Antibacterial effect of 460 nm light-emitting diode in combination with riboflavin against *Listeria monocytogenes* on smoked salmon. *Food Control, 84*, 354–361.

Kang, J. W., Lee, H. Y., & Kang, D. H. (2021). Synergistic bactericidal effect of hot water with citric acid against *Escherichia coli* O157:H7 biofilm formed on stainless steel. *Food Microbiology, 95*, Article 103676.

Kim, J. K., & Harrison, M. A. (2009). Surrogate selection for *Escherichia coli* O157:H7 based on cryotolerance and attachment to romaine lettuce. *Journal of Food Protection, 72*(7), 1385–1391.

Koebmann, B. J., Westerhoff, H. V., Snoep, J. L., Nilsson, D., & Jensen, P. R. (2002). The glycolytic flux in *Escherichia coli* is controlled by the demand for ATP. *Journal of Bacteriology, 184*(14), 3909–3916.

Koo, H., Allan, R. N., Howlin, R. P., Stoodley, P., & Hall-Stoodley, L. (2017). Targeting microbial biofilms: current and prospective therapeutic strategies. *Nature Reviews Microbiology, 15*(12), 740.

Lavoine, N., Givord, C., Tabary, N., Desloges, I., Martel, B., & Bras, J. (2014). Elaboration of a new antibacterial bio-nano-material for food-packaging by synergistic action of cyclodextrin and microfibrillated cellulose. *Innovative Food Science & Emerging Technologies, 26*, 330–340.

Lee, N. Y., Kim, S. W., & Ha, S. D. (2014). Synergistic effects of ultrasound and sodium hypochlorite (NaOCl) on reducing *Listeria monocytogenes* ATCC 19118 in broth, stainless steel, and iceberg lettuce. *Foodborne Pathogens and Disease, 11*(7), 581–587.

Li, J., Ding, T., Liao, X., Chen, S., Ye, X., & Liu, D. (2017). Synergetic effects of ultrasound and slightly acidic electrolyzed water against *Staphylococcus aureus* evaluated by flow cytometry and electron microscopy. *Ultrasonics Sonochemistry, 38*, 711–719.

Liao, X., Li, J., Suo, Y., Chen, S., Ye, X., Liu, D., & Ding, T. (2018). Multiple action sites of ultrasound on *Escherichia coli* and *Staphylococcus aureus*. *Food Science and Human Wellness, 7*(1), 102–109.

Liu, Q., Chen, L., Laserna, A. K. C., He, Y., Feng, X., & Yang, H. (2020). Synergistic action of electrolyzed water and mild heat for enhanced microbial inactivation of *Escherichia coli* O157:H7 revealed by metabolomics analysis. *Food Control, 110*, Article 107026.

Liu, Q., Jin, X., Feng, X., Yang, H., & Fu, C. (2019). Inactivation kinetics of *Escherichia coli* O157:H7 and *Salmonella* Typhimurium on organic carrot (*Daucus carota* L.) treated with low concentration electrolyzed water combined with short-time heat treatment. *Food Control, 106*, Article 106702.

Lu, H., Que, Y., Wu, X., Guan, T., & Guo, H. (2019). Metabolomics deciphered metabolic reprogramming required for biofilm formation. *Scientific Reports, 9*(1), 1–7.

Lushchak, V. I. (2011). Adaptive response to oxidative stress: bacteria, fungi, plants and animals. *Comparative Biochemistry and Physiology Part C: Toxicology & Pharmacology, 153*(2), 175–190.

Luu, P., Chhetri, V. S., Janes, M. E., King, J. M., & Adhikari, A. (2021). Efficacy of gaseous chlorine dioxide in reducing *Salmonella enterica, E. coli* O157:H7, and *Listeria monocytogenes* on strawberries and blueberries. *LWT, 141*, Article 110906.

Nachtigall, C., Berger, C., Kovanović, T., Wefers, D., Jaros, D., & Rohm, H. (2019). Shear induced molecular changes of exopolysaccharides from lactic acid bacteria. *Food Hydrocolloids, 97*, Article 105181.

Nachtigall, C., Rohm, H., & Jaros, D. (2021). Degradation of exopolysaccharides from lactic acid bacteria by thermal, chemical, enzymatic and ultrasound Stresses. *Foods, 10*(2), 396.

National Organic Program. (2011). The use of chlorine materials in organic production and handling. NOP 5026. https://www.ams.usda.gov/sites/default/files/media/5026.pdf Accessed June 6, 2021.

O'Byrne, C. P., & Booth, I. R. (2002). Osmoregulation and its importance to food-borne microorganisms. *International Journal of Food Microbiology, 74*(3), 203–216.

Pang, X., & Yuk, H. G. (2019). Effects of the colonization sequence of *Listeria monocytogenes* and *Pseudomonas fluorescens* on survival of biofilm cells under food-related stresses and transfer to salmon. *Food Microbiology, 82*, 142–150.

Sam, C.-H., & Lu, H.-K. (2009). The role of hypochlorous acid as one of the reactive oxygen species in periodontal disease. *Journal of Dental Sciences, 4*(2), 45–54.

Schalenbach, M., Zeradjanin, A. R., Kasian, O., Cherevko, S., & Mayrhofer, K. J. (2018). A perspective on low-temperature water electrolysis-challenges in alkaline and acidic technology. *International Journal of Electrochemical Science, 13*(2), 1173–1226.

Smart, K. F., Aggio, R. B., Van Houtte, J. R., & Villas-Bôas, S. G. (2010). Analytical platform for metabolome analysis of microbial cells using methyl chloroformate derivatization followed by gas chromatography–mass spectrometry. *Nature Protocols, 5*(10), 1709.

Tan, J., & Karwe, M. V. (2021). Inactivation and removal of *Enterobacter aerogenes* biofilm in a model piping system using plasma-activated water (PAW). *Innovative Food Science & Emerging Technologies, 69*, Article 102664.

Torlak, E., & Sert, D. (2013). Combined effect of benzalkonium chloride and ultrasound against *Listeria monocytogenes* biofilm on plastic surface. *Letters in Applied Microbiology, 57*(3), 220–226.

Valle, J., Da Re, S., Schmid, S., Skurnik, D., d'Ari, R., & Ghigo, J. M. (2008). The amino acid valine is secreted in continuous-flow bacterial biofilms. *Journal of Bacteriology, 190*(1), 264.

Van Der Hooft, J. J., Goldstone, R. J., Harris, S., Burgess, K. E., & Smith, D. G. (2019). Substantial extracellular metabolic differences found between phylogenetically closely related probiotic and pathogenic strains of *Escherichia coli*. *Frontiers in Microbiology, 10*, 252.

Vidra, A., & Németh, Á. (2018). Bio-produced acetic acid: a review. *Periodica Polytechnica, Chemical Engineering, 62*(3), 245–256.

Vyas, N., Manmi, K., Wang, Q., Jadhav, A. J., Barigou, M., Sammons, R. L., … Walmsley, A. D. (2019). Which parameters affect biofilm removal with acoustic cavitation? A review. *Ultrasound in Medicine & Biology, 45*(5), 1044–1055.

Wang, Y., Wu, J. E., & Yang, H. (2022). Comparison of the metabolic responses of eight *Escherichia coli* strains including the "big six" in pea sprouts to low concentration electrolysed water by NMR spectroscopy. *Food Control, 131*, Article 108458.

Wiklund, S. (2008). *Multivariate data analysis for Omics*. Umea: Umetrics.

Wu, J., Zhao, L., Lai, S., & Yang, H. (2021). NMR-based metabolomic investigation of antimicrobial mechanism of electrolysed water combined with moderate heat treatment against *Listeria monocytogenes* on salmon. *Food Control, 125*, Article 107974.

Wu, S., Nie, Y., Zhao, J., Fan, B., Huang, X., Li, X., Sheng, J., Meng, D., Ding, Y., & Tang, X. (2018). The synergistic effects of low-concentration acidic electrolyzed water and ultrasound on the storage quality of fresh-sliced button mushrooms. *Food and Bioprocess Technology, 11*(2), 314–323.

Yang, H. (2012). *Evaluating the antimicrobial mechanism of neutral electrochemically activated water on foodborne pathogens and their biofilms*. University of Minnesota. Dissertation/Thesis.

Yang, L., Mih, N., Anand, A., Park, J. H., Tan, J., Yurkovich, J. T., … Seo, S. W. (2019). Cellular responses to reactive oxygen species are predicted from molecular mechanisms. *Proceedings of the National Academy of Sciences, 116*(28), 14368–14373.

Yemmireddy, V. K., & Hung, Y. C. (2015). Effect of binder on the physical stability and bactericidal property of titanium dioxide (TiO2) nanocoatings on food contact surfaces. *Food Control, 57*, 82–88.

Yu, H., Liu, Y., Li, L., Guo, Y., Xie, Y., Cheng, Y., & Yao, W. (2020). Ultrasound-involved emerging strategies for controlling foodborne microbial biofilms. *Trends in Food Science & Technology, 96*, 91–101.

Zeng, X., Tang, W., Ye, G., Ouyang, T., Tian, L., Ni, Y., & Li, P. (2010). Studies on disinfection mechanism of electrolyzed oxidizing water on *E. coli* and *Staphylococcus aureus*. *Journal of Food Science, 75*(5), M253–M260.

Zhang, H., Pang, X., Seck, H. L., & Zhou, W. (2021). Low-energy X-ray inactivation of *Listeria monocytogenes* in mono−/co-culture biofilms with *Pseudomonas fluorescens* on food contact surfaces. *Food Microbiology, 103841*.

Zhang, Y., Swart, C., Alseekh, S., Scossa, F., Jiang, L., Obata, T., … Fernie, A. R. (2018). The extra-pathway interactome of the TCA cycle: expected and unexpected metabolic interactions. *Plant Physiology, 177*(3), 966–979.

Zhao, L., Li, S., & Yang, H. (2021). Recent advances on research of electrolyzed water and its applications. *Current Opinion in Food Science, 41*, 180–188.

Zhao, L., Zhang, Y., & Yang, H. (2017). Efficacy of low concentration neutralised electrolysed water and ultrasound combination for inactivating *Escherichia coli* ATCC 25922, *Pichia pastoris* GS115 and *Aureobasidium pullulans* 2012 on stainless steel coupons. *Food Control, 73*, 889–899.

Zhao, L., Zhao, M. Y., Phey, C. P., & Yang, H. (2019). Efficacy of low concentration acidic electrolysed water and levulinic acid combination on fresh organic lettuce (*Lactuca sativa* Var. *Crispa* L.) and its antimicrobial mechanism. *Food Control, 101*, 241–250.

Zhao, L., Zhao, X., Wu, J. E., Lou, X., & Yang, H. (2019). Comparison of metabolic response between the planktonic and air-dried *Escherichia coli* to electrolysed water combined with ultrasound by ^{1}H NMR spectroscopy. *Food Research International, 125*, Article 108607.

Zhao, X., Chen, L., Zhao, L., He, Y., & Yang, H. (2020). Antimicrobial kinetics of nisin and grape seed extract against inoculated *Listeria monocytogenes* on cooked shrimps: survival and residual effects. *Food Control, 115*, Article 107278.